

Morphology Transition from Dendrites to Equiaxed Grains for AlCoCrFeNi High-Entropy Alloys by Copper Mold Casting and Bridgman Solidification

Y. ZHANG, S.G. MA, and J.W. QIAO

The AlCoCrFeNi high-entropy alloys (HEAs) were prepared by the copper mold casting and Bridgman solidification. X-ray diffraction (XRD) results verify that the main phase was body-centered-cubic (bcc) solid solution by these two solidification processes, indicating its good phase stability. Interestingly, the metallographic photos show a morphology transition from dendrites to equiaxed grains after Bridgman solidification, which was considered to have a strong dependence on the parameter of the G/V (the temperature gradient to the growth rate ratio). Compared to the as-cast sample, the plasticity of alloys synthesized by Bridgman solidification was improved by a maximum of 35 pct.

DOI: 10.1007/s11661-011-0981-8

© The Minerals, Metals & Materials Society and ASM International 2011

I. INTRODUCTION

RECENTLY, high-entropy alloys (HEAs) have attracted increasing attention. As the entropy of solid solutions is usually higher than that of intermetallics, which can greatly lower the Gibbs free energy of the system. Thus, the alloys with high entropy of mixing mainly form face-centered-cubic or body-centered-cubic (bcc) solid solutions.^[1-4]

At present, the arc melting and copper mold casting are usually used for the preparation of HEAs,^[5-15] during which the solidification process cannot be easily controlled, which leads to a changing microstructure from the surface to the center of the samples, *e.g.*, inhomogeneous distribution of the dendrites. Furthermore, the undercooled liquid metals have to withstand tensile stress in the suction casting process, which causes the defects of the prepared samples, such as the pores due to the volume shrinking during solidification.

Compared to the copper mold casting, the direction of the thermal conduction and extraction for rod-shape samples obtained by Bridgman solidification is mainly along the longitudinal direction, and the temperature gradient and growth rates can be precisely controlled by adjusting the heating power and withdrawal velocities. For instance, the Al-Cu alloys,^[16] TiAl-based alloys,^[17] and Ni-based superalloys^[18] were prepared and optimized by Bridgman solidification. It was reported that dendrites/bulk-metallic-glass (BMG) composites were successfully tailored by Bridgman solidification, during

which the dendrites are homogeneously distributed within the BMG matrix, and the dendrite spanning length has a strong dependence on the temperature gradient and growth rates.^[19-21]

In this study, the microstructure and mechanical properties of the AlCoCrFeNi HEAs were investigated by these two solidification techniques.

II. EXPERIMENTAL PROCEDURE

Ingots with a nominal composition of AlCoCrFeNi (molar ratio) were prepared by arc melting the mixture of Al, Co, Cr, Fe, and Ni with purity higher than 99.5 wt pct under a Ti-gettered argon atmosphere. In order to ensure the compositional homogeneity, the alloys were remelted at least 4 times. Afterward, the ingots were divided into two parts. One part was remelted and then cast into cylindrical rods with diameters of 3 and 5 mm. The cross sections of the samples were etched with the aqua regia solution, and the microstructures were investigated by metallographic microscope. Another part was crashed into pieces and placed in an alumina tube with an internal diameter of 3 mm and a wall thickness of ~1 mm. Then the samples were inductively heated to melt by adjusting the heating power, holding for 15 minutes. Bridgman solidification was carried out with withdrawal velocities of 200 to 1800 $\mu\text{m/s}$ through a temperature gradient of ~70 K/mm into the water-cooled Ga-In-Sn liquid alloys, a schematic diagram of which can be obtained in Reference 22. The phases of the samples were analyzed by X-ray diffraction (XRD) in a PHILIPS* APD-10 diffractom-

Y. ZHANG, Professor, and S.G. MA, Postdoctoral Candidate, are with the State Key Laboratory for Advanced Metals and Materials, University of Science & Technology Beijing, Beijing 100083, P.R. China. Contact e-mail: drzhangy@ustb.edu.cn J.W. QIAO, Associate Professor, is with the College of Materials Science and Engineering, Taiyuan University of Technology, Taiyuan 030024, P.R. China.

Manuscript submitted April 28, 2011.

Article published online November 15, 2011

*PHILIPS is a trademark of FEI Company, Hillsboro, OR.

eter (Cu K_{α} radiation). The uniaxial compressive tests were performed on 6-mm-long sections cut from the

3-mm-diameter cylinders by using an MTS 809 materials testing machine at room temperature with a strain rate of $2 \times 10^{-4} \text{ s}^{-1}$. The microstructure morphologies of the longitudinal sections were investigated by the

metallographic microscope and the scanning electron microscope (SEM) equipped with an energy-dispersive X-ray spectrometer.

III. RESULTS

A. XRD Analysis

The XRD patterns, as shown in Figure 1, are taken on the longitudinally sectioned specimens obtained by the copper mold casting and Bridgman solidification. It is apparent that all the samples have similar bcc reflections and no obvious lattice-constant changes of bcc solid solutions. The lattice-constant parameter is estimated to be on the order of $0.2890 \pm 0.0005 \text{ nm}$ from the strongest (110) peak, indicating good phase and structure stabilities. This may be ascribed to the unique high-entropy effect for HEAs.^[3]

B. Microstructure Evolution

The metallographic photos of as-cast samples obtained by the copper mold casting are displayed in Figure 2. Flowery dendrites can be seen in Figures 2(a) and (b), for the central region of the samples with diameters of 3 and 5 mm, respectively. The dendrites are

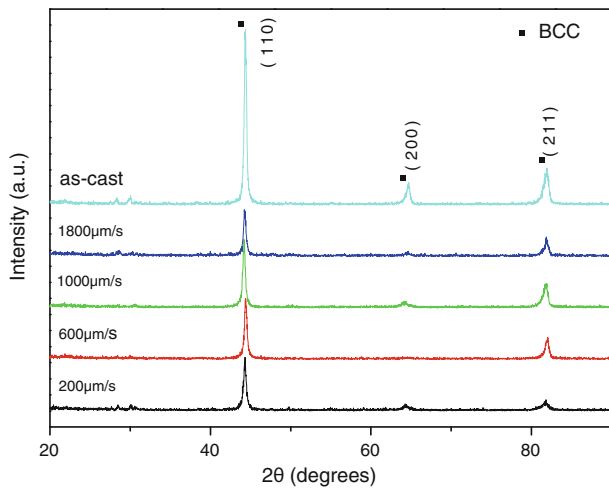


Fig. 1—XRD patterns of AlCoCrFeNi HEAs of as-cast and Bridgman solidification with various withdrawal velocities of 200 to $1800 \mu\text{m/s}$.

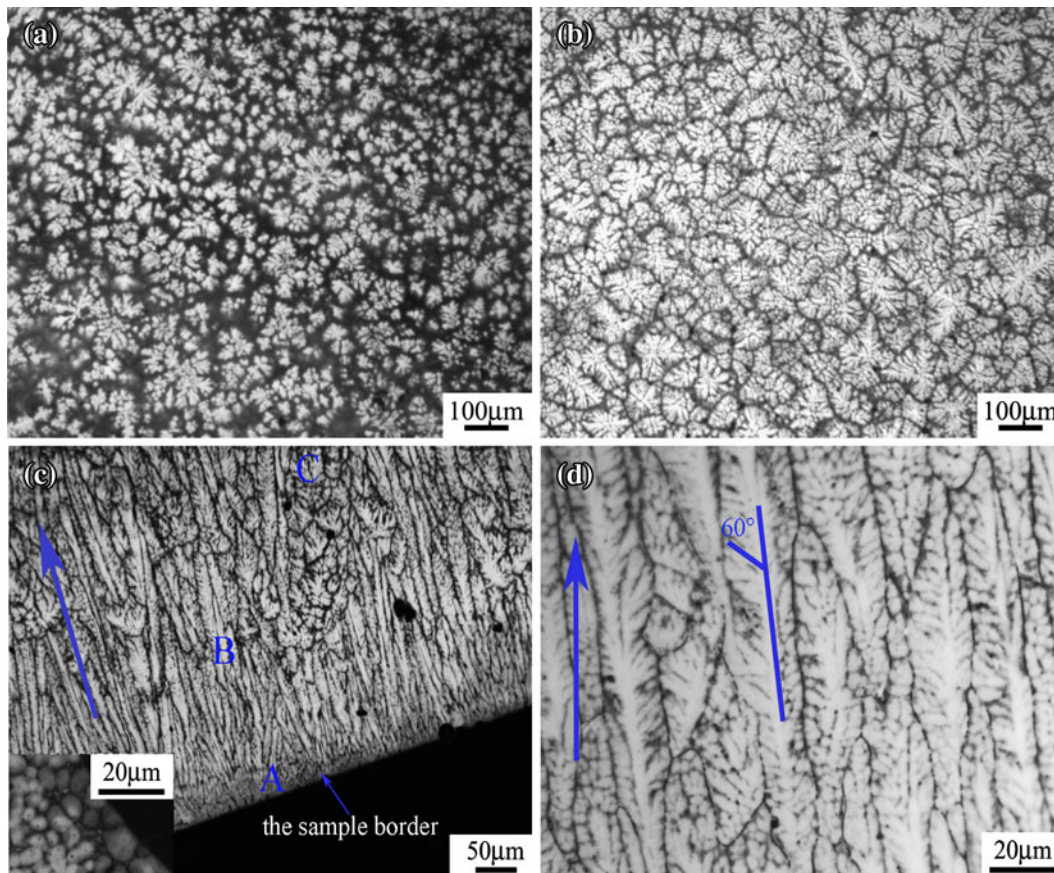


Fig. 2—Metallographic photos of AlCoCrFeNi HEA cylindrical rods by copper mold suction casting: (a) and (b) dendrites viewed in the central region of the samples with diameters of 3 and 5 mm, respectively; (c) typical casting microstructures and the inset is a magnification of the finely equiaxed grains close to the sample border; and (d) morphology of the columnar dendrites corresponding to the B location in (c).

intensively embedded on the grain matrix and surrounded by the grain boundary. The average spanning length of dendrites is in the range of 50 to 100 μm , and the growth of branched dendrites starts from a common center into arbitrary directions. Figures 2(c) and (d) present the typical microstructures of as-cast samples with the diameter of 5 mm, and the solidification direction is indicated by an arrow: the outermost are finely equiaxed grains originating from the large cooling rate, which are clearly seen in the inset of Figure 2(c), and the grain size is about 5 to 10 μm ; the intermediates are carrotlike columnar dendrites, which grow along a preferred orientation; and the innermost are thick equiaxed dendrites (points labeled A, B, and C, respectively). In particular, Figure 2(d) displays the morphology of the columnar dendrites corresponding to the B location in Figure 2(c). Clearly, most of the primary dendrite trunks, inclined to an angle of about 10 to 20 deg with respect to the vertical, are aligned along a specific crystallographic direction. The side arms of the dendrites that developed on the left side of the primary dendrite trunks usually have an angle of about 60 deg with respect to the trunks. This can also be observed in the dendrites growth morphologies of a unidirectionally solidified Al-9 pct Si alloy.^[23]

Figure 3 shows the metallographic photos of the longitudinal sections of the solidified rods by Bridgman

solidification with withdrawal velocities of 200 to 1800 $\mu\text{m/s}$. Interestingly, after Bridgman solidification, the morphologies are equiaxed grains rather than flowery dendrites, as shown in Figures 3(a) through (d), and the grain boundary is indicated by the arrow and marked GB in Figure 3(a). The statistical analyses reveal that there is no obvious change for the average grain size (about 100 to 150 μm) in Figures 3(a) through (d). This suggests that the AlCoCrFeNi HEA is not sensitive to these withdrawal velocities, which may be due to the sluggish diffusion effect of solute atoms that impairs the growth of the grains during solidification.^[24]

Furthermore, the secondary electron images of the longitudinal sections of the solidified rods by Bridgman solidification are exhibited in Figure 4. Figures 4(a), (b), (c), and (d) correspond to the withdrawal velocity of 200, 600, 1000, and 1800 $\mu\text{m/s}$, respectively. Figures 4(e) and (f) are the magnifications of the grain matrix for withdrawal velocities of 200 and 1800 $\mu\text{m/s}$, respectively. The grain boundaries are clearly seen in Figures 4(a) through (d), and the angle of the intersection of two grain boundaries is about 120 deg. Moreover, the microstructure of the grain matrix of Figure 4(a) is distinctly different from that of Figures 4(b) through (d). More detailed observations are displayed in Figures 4(e) and (f). Coherent and alternating platelets, with different sizes of ~150 to 400 nm in length and 100 to 200 nm in

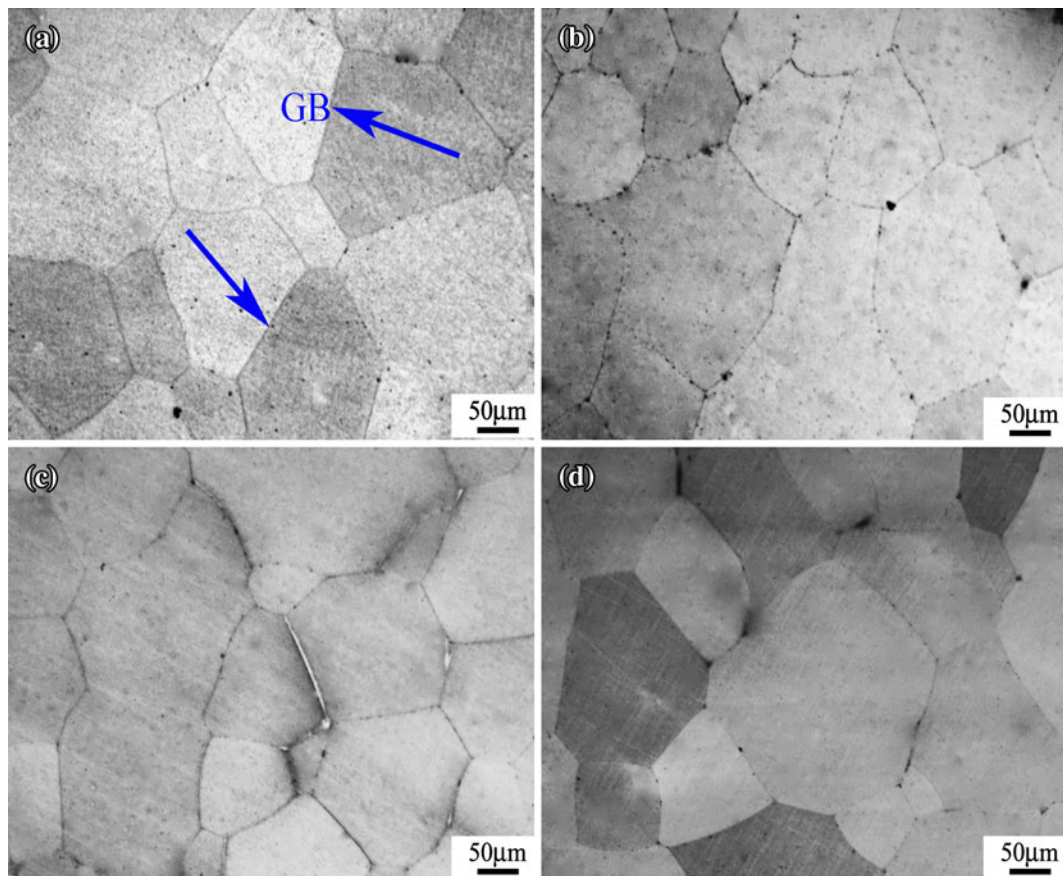


Fig. 3—Metallographic photos of AlCoCrFeNi HEAs by Bridgman solidification with withdrawal velocities of (a) 200, (b) 600, (c) 1000, and (d) 1800 $\mu\text{m/s}$.

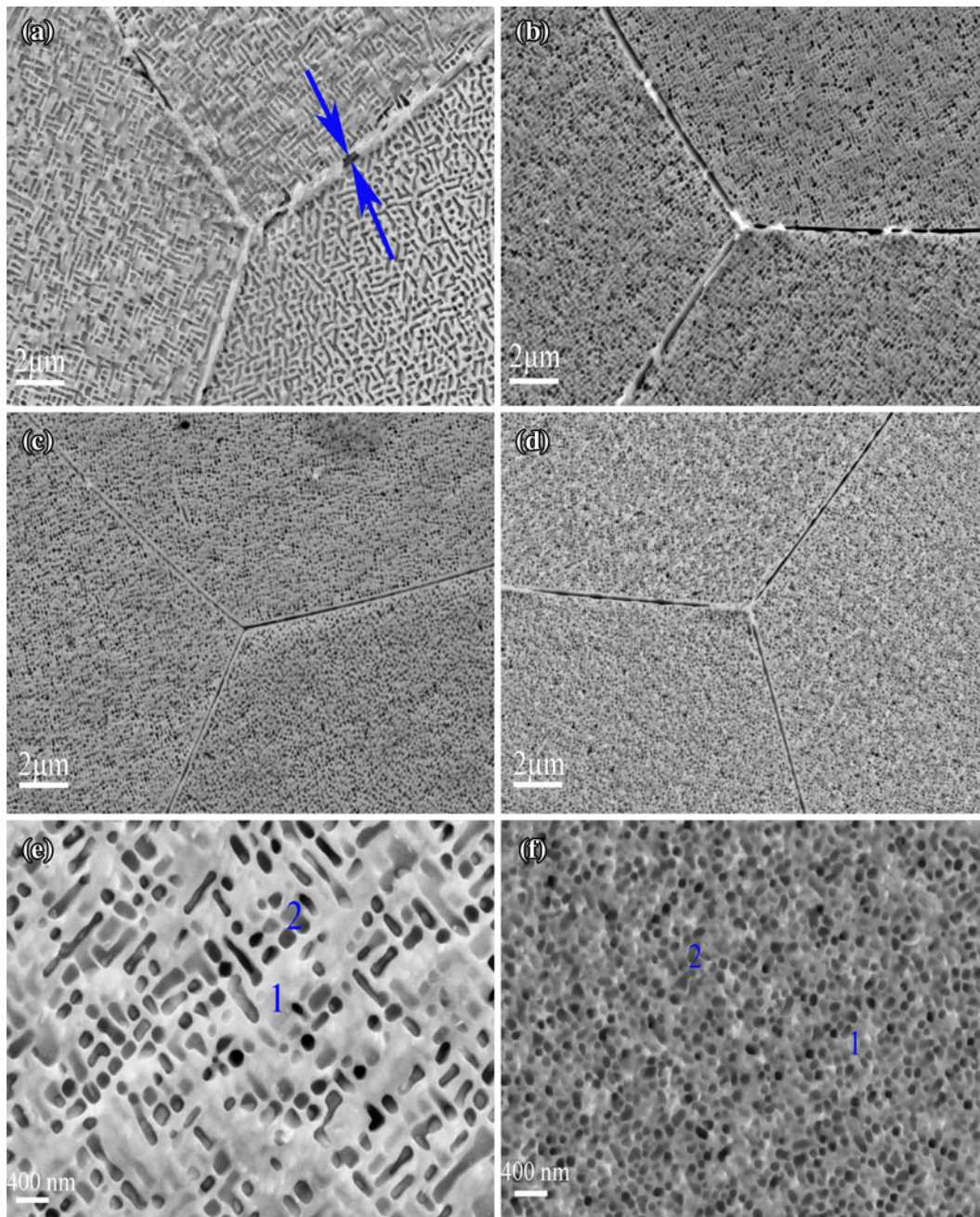


Fig. 4—SEM secondary electron images of AlCoCrFeNi HEAs by Bridgman solidification with withdrawal velocities of (a) 200, (b) 600, (c) 1000, and (d) 1800 $\mu\text{m/s}$. (e) and (f) magnifications of (a) and (d), respectively.

width, can be seen in Figure 4(e), and such similar structures were reported in the Fe-Ni-Mn-Al alloy systems.^[25] On the other hand, honeycomb-like structure with uniform dispersion of spherical particles can be seen in Figure 4(f), and the size of the nanoscale spherical precipitations is about 50 to 100 nm. These nanoscale precipitations may originate from the spinodal decomposition, leading to a modulated structure composed of ordered (B2) and disordered (A2) phases, respectively. This decomposition was also reported in the AlCuCoCrFeNi alloy systems,^[3] and was further confirmed by using the high-energy X-ray beam measurement in Reference 26.

C. Mechanical Properties

The compressive engineering stress-strain curves of the solidified rods synthesized by the copper mold casting and Bridgman solidification are displayed in Figure 5. The plastic strain limits of alloys were improved to some extent by Bridgman solidification compared to the as-cast sample, especially at the withdrawal velocity of 1800 $\mu\text{m/s}$ (up to 30 pct). The yielding strengths of alloys are evidently lower than that of the as-cast sample, and have no distinct change under different withdrawal velocities, as shown in Table I. This may be ascribed to the fact that the disappearance of the

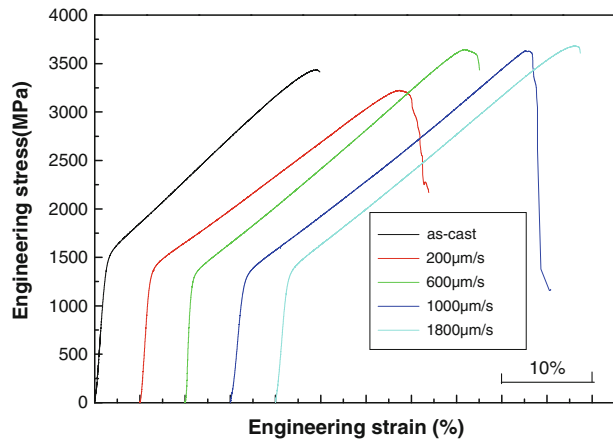


Fig. 5—Compressive engineering stress-strain curves of AlCoCrFeNi HEAs by the copper mold suction casting and Bridgman solidification with various withdrawal velocities of 200 to 1800 $\mu\text{m/s}$.

Table I. Mechanical Properties of AlCoCrFeNi Alloys by Copper Mold Casting and Bridgman Solidification with Various Withdrawal Velocities of 200 to 1800 $\mu\text{m/s}$

Alloys	$\sigma_{0.2}$ (MPa)	σ_{max} (MPa)	ϵ_p (Pct)
As cast	1451	3440	21.6
200 $\mu\text{m/s}$	1312	3228	26.1
600 $\mu\text{m/s}$	1263	3629	28.6
1000 $\mu\text{m/s}$	1275	3629	28.7
1800 $\mu\text{m/s}$	1288	3669	29.5

dendrites and more homogeneous microstructure facilitate the movement of the dislocations. In addition, with the increase of the withdrawal velocity, the microstructure of the grain matrix becomes finer and more uniform, as indicated in Figure 4, and the nanoscale spherical precipitation enables the release of the stress caused by the pileup of the dislocations and the absorption of the external energy during plastic deformation, and delays the propagation of the cracks, which improves the plasticity of alloys. Besides, less constitutional segregation along grain boundaries also has a positive contribution.

IV. DISCUSSION

A. Morphology Transition Mechanism

The morphology has a strong dependence on the parameter of the G/V during solidification, in which G is the temperature gradient and V is the growth rate. With the increase of the G/V , which leads to a smaller constitutional supercooling, the microstructure morphologies will change from dendrites to columnar or cellular crystals, and to equiaxed grains.^[27] Accordingly, for the copper mold casting, the temperature gradient close to the sample border is almost regarded as the infinite, whereas the G in the central region is close to the zero; on the other hand, the growth rate remains very large from the surface to the center (the formation of the microstructure is almost instantaneously accomplished), together producing a distinctly different value of the G/V along the radial

direction of the sample, which is favorable to the formation of the dendrite segregation region and further produces an inhomogeneous microstructure, as shown in Figure 2. However, for Bridgman solidification, the temperature gradient in the liquid/solid interface front is almost a constant of ~ 70 K/mm, and the growth rate can be roughly considered to be the withdrawal velocities of 200 to 1800 $\mu\text{m/s}$ (generally, the growth rate is always lower than the withdrawal velocity), which is much lower than that of the as cast. As a result, a larger value of the G/V enables the formation of the equiaxed grains.

In addition, the heating temperature by Bridgman solidification is lower than that by arc melting. As a result, the dendrites of smaller arm spacing may be remelted and disappear, while the dendrites of larger arm spacing may coarsen or spheroidize due to lower surface energy and a longer holding time.^[28]

B. Stability of the Grain Size After Bridgman Solidification

The growth of the grain is due to the migration of the interface between two grains or the driving force originating from the difference of the interface curvature radius. For a solid solution, to keep the stability of the grain size, a qualitative expression can be as follows:

$$\sigma_A / \sin A = \sigma_B / \sin B = \sigma_C / \sin C \quad [1]$$

in which A , B , and C are the angle of the intersection of two adjacent grain boundaries, respectively; σ_A , σ_B , and σ_C are the interface tensions on the grain boundaries, respectively; and $\sin A$, $\sin B$, and $\sin C$ are the sine values of the corresponding angle, respectively. Here, it can be assumed that $\sigma_A = \sigma_B = \sigma_C$ for the present alloy of a solid solution; furthermore, A , B , and C should be equal to 120 deg. The flat interface corresponds to the infinite curvature radius and the driving force of zero that facilitate the stability of the grain size. As referenced in Section III-B, the angle of the intersection of two grain boundaries after Bridgman solidification is about 120 deg, and the grain boundary is almost flat, which may be the reason that the grain size has no obvious change under different withdrawal velocities.

V. CONCLUSIONS

The AlCoCrFeNi HEAs are mainly composed of a bcc solid solution phase by copper mold casting and Bridgman solidification. However, the morphology changes from dendrites to equiaxed grains in this alloy after Bridgman solidification, which may be due to the lower heating temperature, longer holding time, and higher G/V values for the Bridgman solidification. The plasticity of alloys was improved to some extent by Bridgman solidification.

ACKNOWLEDGMENTS

The authors are grateful to the program of the National Natural Science Foundation of China

(NNSFC) (Contract No. 5097101) and the support from the State Key Laboratory of Metastable Materials Science and Technology, Yanshan University, Qinhuang Island, China (Contract No. 201103).

REFERENCES

1. G.L. Chen and C.T. Liu: *Int. Mater. Rev.*, 2001, vol. 46, pp. 253–60.
2. B. Cantor, I.T.H. Chang, P.K. Night, and A.J. Vincent: *Mater. Sci. Eng. A*, 2004, vols. 375–377, pp. 213–18.
3. J.W. Yeh, S.K. Chen, S.J. Lin, J.Y. Gan, T.S. Chin, T.S. Shun, C.H. Tsau, and S.Y. Chang: *Adv. Eng. Mater.*, 2004, vol. 6, pp. 299–303.
4. X.F. Wang, Y. Zhang, Y. Qiao, and G.L. Chen: *Intermetallics*, 2007, vol. 15, pp. 357–62.
5. Y.J. Zhou, Y. Zhang, Y.L. Wang, and G.L. Chen: *Appl. Phys. Lett.*, 2007, vol. 90, pp. 181904-1-3.
6. Y.P. Wang, B.S. Li, M.X. Ren, C. Yang, and H.Z. Fu: *Mater. Sci. Eng. A*, 2008, vol. 491, pp. 154–58.
7. L.H. When, H.C. Kou, J.S. Li, H. Chang, X.Y. Xue, and L. Zhou: *Intermetallics*, 2009, vol. 17, pp. 266–69.
8. F.J. Wang, Y. Zhang, and G.L. Chen: *J. Eng. Mater. Technol.*, 2009, vol. 131, pp. 034501-1-3.
9. C.W. T, Y.L. Chen, M.H. Tsai, J.W. Yeh, T.T. Shun, and S.K. Chen: *J. Alloy Compd.*, 2009, vol. 486, pp. 427–35.
10. Z.H. Hu, Y.Z. Zhan, G.H. Zhang, J. She, and C.H. Li: *Mater. Des.*, 2010, vol. 31, pp. 1599–1602.
11. T.T. Shun, C.H. Hung, and C.F. Lee: *J. Alloy Compd.*, 2010, vol. 495, pp. 55–58.
12. S. Singh, N. Wanderka, B.S. Murty, U. Glatzel, and J. Banhart: *Acta Mater.*, 2011, vol. 59, pp. 182–90.
13. J.M. Zhu, H.M. Fu, H.F. Zhang, A.M. Wang, H. Li, and Z.Q. Hu: *Mater. Sci. Eng. A*, 2010, vol. 527, pp. 6975–79.
14. J.M. Zhu, H.M. Fu, H.F. Zhang, A.M. Wang, H. Li, and Z.Q. Hu: *Mater. Sci. Eng. A*, 2010, vol. 527, pp. 7210–14.
15. C. Li, J.C. Li, M. Zhao, and Q. Jiang: *J. Alloy Compd.*, 2010, vol. 504S, pp. S516–18.
16. J.D. Hunt: *Mater. Sci. Eng.*, 1984, vol. 64, pp. 75–83.
17. P.N. Quedest and M. Mclean: *Mater. Sci. Eng.*, 1984, vol. 65, pp. 171–80.
18. J. Lapin and Z. Galalová: *Intermetallics*, 2011, vol. 19, pp. 797–804.
19. J.W. Qiao, Y. Zhang, and P.K. Liaw: *Adv. Eng. Mater.*, 2008, vol. 10, pp. 1039–42.
20. J.W. Qiao, S. Wang, Y. Zhang, P.K. Liaw, and G.L. Chen: *Appl. Phys. Lett.*, 2009, vol. 94, pp. 151905-1-3.
21. J.W. Qiao, A.C. Sun, E.W. Huang, Y. Zhang, P.K. Liaw, and C.P. Chuang: *Acta Mater.*, 2011, vol. 59, pp. 4126–37.
22. L. Hu, B.Y. Liu, F. Ye, B.C. Wei, and G.L. Chen: *Intermetallics*, 2011, vol. 19, pp. 662–65.
23. S. Henry, T. Minghetti, and M. Rappaz: *Acta Mater.*, 1998, vol. 18, pp. 6440–43.
24. J.W. Yeh: *Ann. Chim. Sci. Mater.*, 2006, vol. 31, pp. 633–48.
25. J.A. Hanna, I. Baker, M.W. Wittmann, and P.R. Munroe: *J. Mater. Res.*, 2005, vol. 20, pp. 791–95.
26. J.W. Qiao, S.G. Ma, E.W. Huang, C.P. Chuang, P.K. Liaw, and Y. Zhang: *Mater. Sci. Forum*, 2011, vol. 668, pp. 419–25.
27. A. Ludwig, I. Wager, J. Laakmann, and P.R. Sahn: *Mater. Sci. Eng. A*, 1994, vol. 178, pp. 299–303.
28. S. Terzi, L. Salvo, M. Suery, A.K. Dahle, and E. Boller: *Acta Mater.*, 2010, vol. 58, pp. 20–30.